Electronic Supplementary Information

Dominant dimer emission provides colour stability for red thermally activated delayed fluorescence emitter

Tom Cardeynaels,[a,b] Marc K. Etherington,[c,d,*] Simon Paredis,[a] Andrei S. Batsanov,[e] Jasper Deckers,[a] Kleitos Stavrou,[d] Dirk Vanderzande,[a] Andrew P. Monkman,[d] Benoît Champagne[b] and Wouter Maes[a,*]

[a] Hasselt University, Institute for Materials Research (IMO-IMOMEC), Design & Synthesis of Organic Semiconductors (DSOS), Agoralaan 1, 3590 Diepenbeek, Belgium and IMOMEC Division, IMEC, Wetenschapspark 1, 3590 Diepenbeek, Belgium
[b] University of Namur, Laboratory of Theoretical Chemistry, Theoretical and Structural Physical Chemistry Unit, Namur Institute of Structured Matter, Rue de Bruxelles 61, 5000 Namur, Belgium
[c] Department of Mathematics, Physics & Electrical Engineering, Northumbria University, Ellison Place, Newcastle upon Tyne, NE1 8ST, United Kingdom
[d] OEM group, Department of Physics, Durham University, South Road, Durham DH1 3LE, United Kingdom
[e] Department of Chemistry, Durham University, South Road, Durham DH1 3LE, United Kingdom

Table of contents

1. Experimental details

1.1 Materials and methods

All reagents and chemicals were obtained from commercial sources and used without further purification. Dry solvents were obtained using an MBraun solvent purification system (MB SPS-800) equipped with alumina columns. Preparative (recycling) size exclusion chromatography (SEC) was performed on a JAI LC-9110 NEXT system equipped with JAIGEL 1H and 2H columns (eluent chloroform, flow rate 3.5 mL min^{-1}). Proton and carbon nuclear magnetic resonance (^{1}H and ^{13}C NMR) spectra were obtained on a Jeol spectrometer operating at 400 MHz for ^{1}H (100 MHz for ^{13}C). Chemical shifts (δ) are given in ppm relative to $CDCl_3$ (δ = 7.26 ppm for ^{1}H NMR, δ = 77.06 ppm for ^{13}C NMR). All NMR spectra were taken at room temperature. Matrix-assisted laser desorption/ionization - time-of-flight (MALDI-ToF) mass spectra were recorded on a Bruker Daltonics UltrafleXtreme ToF/ToF. Approximately 10 µL of the matrix solution (25 mg mL^{-1} *trans*-2-[3-(4-*tert*-butylphenyl)-2-methyl-2-propenylidene]malononitrile (DTCB) in chloroform) was mixed with 3 µL of the analyte solution (10 mg mL^{-1} In chloroform), after which 0.5 µL of the resulting solution was spotted onto an MTP Anchorchip 600/384 MALDI plate. All solution-based steady state absorption and emission spectra were recorded on a UV-3600 double beam spectrophotometer (Shimadzu) and a Fluoromax fluorimeter (Jobin Yvon), respectively. All spectroscopic measurements were done in spectroscopic grade solvents. Films were prepared via drop-casting using a mixture of the emitter and host in chloroform at the designated concentrations. The films were drop-cast onto a quartz substrate at 65 °C to facilitate evaporation of the solvent. Steady state absorption and emission spectra of the films were collected using a UV-3600 double beam spectrophotometer (Shimadzu) and a Fluoromax fluorimeter (Jobin Yvon), respectively. Time-resolved photoluminescence spectra and decays were recorded using a nanosecond gated spectrograph-coupled iCCD (Stanford) using an Nd:YAG laser emitting at 355 nm (EKSPLA). Laser power experiments were conducted using an N_2 laser (Lasertechnik Berlin) emitting at 337 nm with the same nanosecond gated spectrograph-coupled iCCD (Stanford) camera, attenuating the excitation using reflective neutral density filters. The absolute PLQY measurements were performed using 365 nm excitation from an Ocean Optics LLS-LED and an integrating sphere connected to an Ocean Optics QePro Spectrometer. 1,3-Diphenylisobenzofuran (1,3-DPBF) was used as a singlet oxygen ($^{1}O_2$) scavenger to determine the singlet oxygen quantum yields (Φ_Δ). The $^{1}O_2$ production was monitored by following the absorbance of 1,3-DPBF at 414 nm upon excitation at 325 nm. The average Φ_Δ was calculated from three independent measurements. To determine Φ_Δ, a relative method was used according to Equation (1). Here, *x* and *st* represent the sample and the standard, respectively. Φ, A, m, and n represent the singlet oxygen quantum yield, the absorbance at the excitation wavelength (λ_{exc} = 325 nm), the slope of the decrease in absorbance of 1,3-DPBF over time, and the refractive index of the solvent used for the measurement, respectively. Optically matched solutions with an absorbance around 0.6 at 414 nm and 0.3 at λ_{exc} were used. Coronene (λ_{exc} = 325 nm, Φ_Δ = 0.9) in spectrograde toluene was used as a standard.[1, 2] All solutions were continuously stirred during all measurements using a Cimarec i magnetic stirrer.

$$\Phi_x = \Phi_{st}\left(\frac{1-10^{-A_{st}}}{1-10^{-A_x}}\right)\left(\frac{m_x}{m_{st}}\right)\left(\frac{n_x}{n_{st}}\right)^2 \quad (1)$$

X-ray diffraction experiments were carried out on a Bruker 3-circle D8 Venture diffractometer with a PHOTON III 14 MM CPAD area detector, using Mo-K_α radiation (λ=0.71073 Å) from an Incoatec IµS microsource with focusing mirrors. Crystals were cooled using a Cryostream (Oxford Cryosystems) open-flow N_2 gas cryostat. The structures were solved by a dual-space intrinsic phasing method using the SHELXT 2018/2 program,[3] and refined by full-matrix least squares using SHELXL 2018/3 software[4] on an OLEX2 platform.[5]

1.2 Synthesis procedures

4H-Dithieno[3,2-b:2',3'-d]pyrrole (DTP)

For the synthesis of DTP, several methods have been reported.[6, 7] Förtsch *et al.* compared several synthetic pathways and developed a single-step synthesis using triphenylsilylamine as the ring-closing reagent.[6] The intermediate triphenylsilyl-protected DTP is not retrieved and instead the reaction proceeds directly to the unprotected DTP in high yields of around 72%. However, after several attempts, no product could be obtained under these conditions in our hands and even changing the catalytic system to $Pd_2(dba)_3$-(tBu)$_3$PH(BF_4) did not lead to the formation of the desired product. Instead, the two-step procedure as reported in ref. 7 has been used.

*2,4,5,6-tetrakis(4H-dithieno[3,2-b:2',3'-d]pyrrol-4-yl)isophthalonitrile (**4DTPIPN**)*

NaH (60% in oil; 105.1 mg, 2.63 mmol) was added slowly to a stirred solution of DTP (455.7 mg, 2.54 mmol; 5 eq.) in dry THF under nitrogen atmosphere at room temperature. After 10 min, tetrafluoroterephthalonitrile (101.6 mg, 0.51 mmol) was added and the reaction mixture was stirred for 16 h at 50 °C in an oil bath. Thereafter, the excess of NaH was quenched with water (0.5 mL). The resulting solid was filtered off, washed with water and EtOH, and dried under vacuum. **4DTPIPN** was obtained as a yellow solid (388.0 mg, 91%). Additional purification was performed using preparative (recycling) size exclusion chromatography before photophysical analysis. ^{1}H NMR (400 MHz, $CDCl_3$): 7.43 (d, J = 5.4 Hz, 2H), 7.28 (d, J = 5.4 Hz, 2H), 6.98 (d, J = 5.4 Hz, 4H), 6.69 (d, J = 5.4 Hz, 2H), 6.62 (d, J = 5.4 Hz, 4H), 6.04 (d, J = 5.4 Hz, 2H). ^{13}C NMR (100 MHz, $CDCl_3$): 144.92, 143.99, 143.39, 142.50, 141.77, 130.29, 125.27, 124.51, 123.77, 120.21, 119.88, 118.75, 111.97, 111.79, 110.93, 109.24. MS (MALDI-ToF) Calcd. for $C_{40}H_{16}N_6S_8$ $[M]^+$: *m/z* 835.920, found: 835.926.

2. NMR spectra

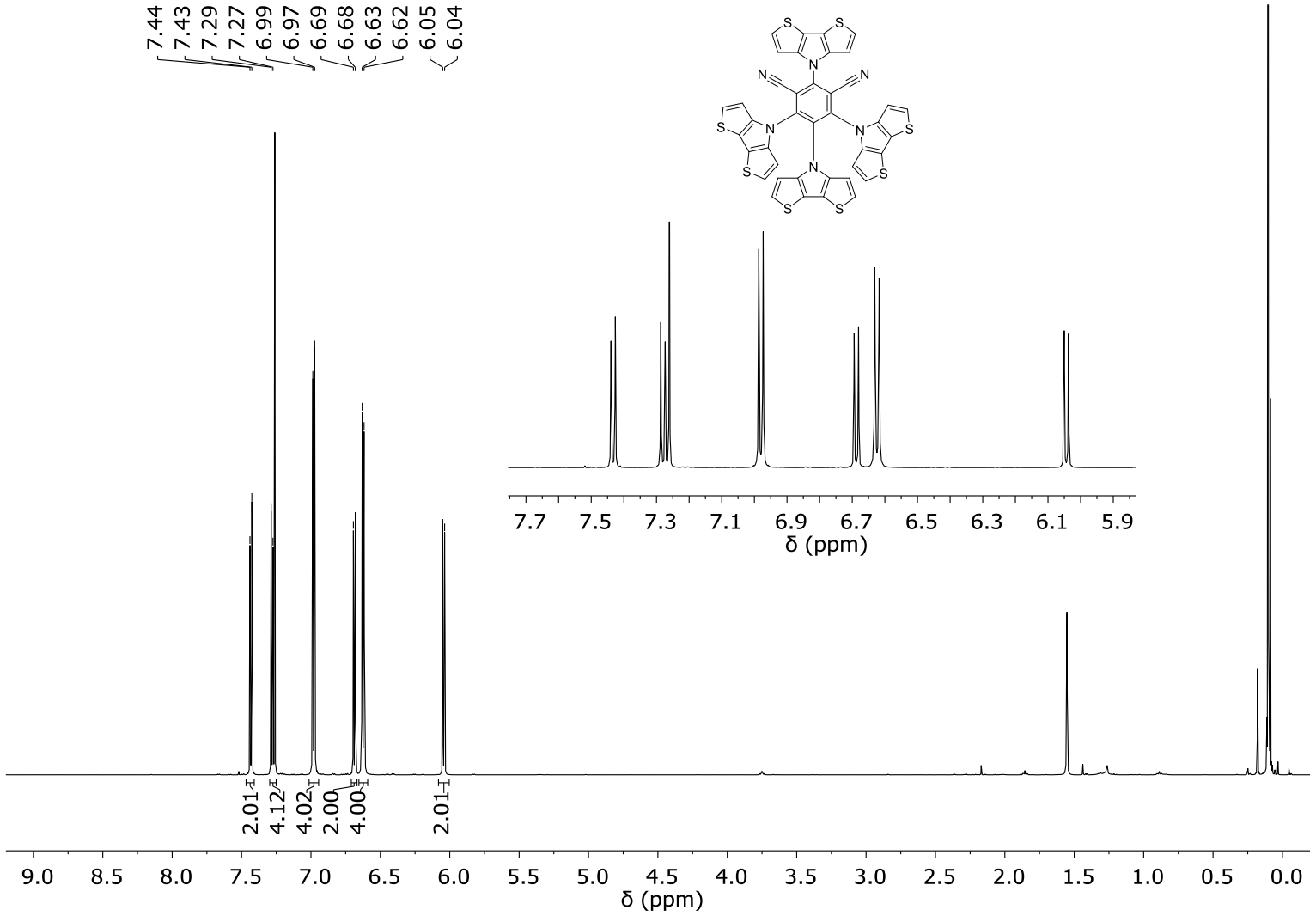

Figure S1: ^{1}H NMR spectrum of **4DTPIPN** in $CDCl_3$.

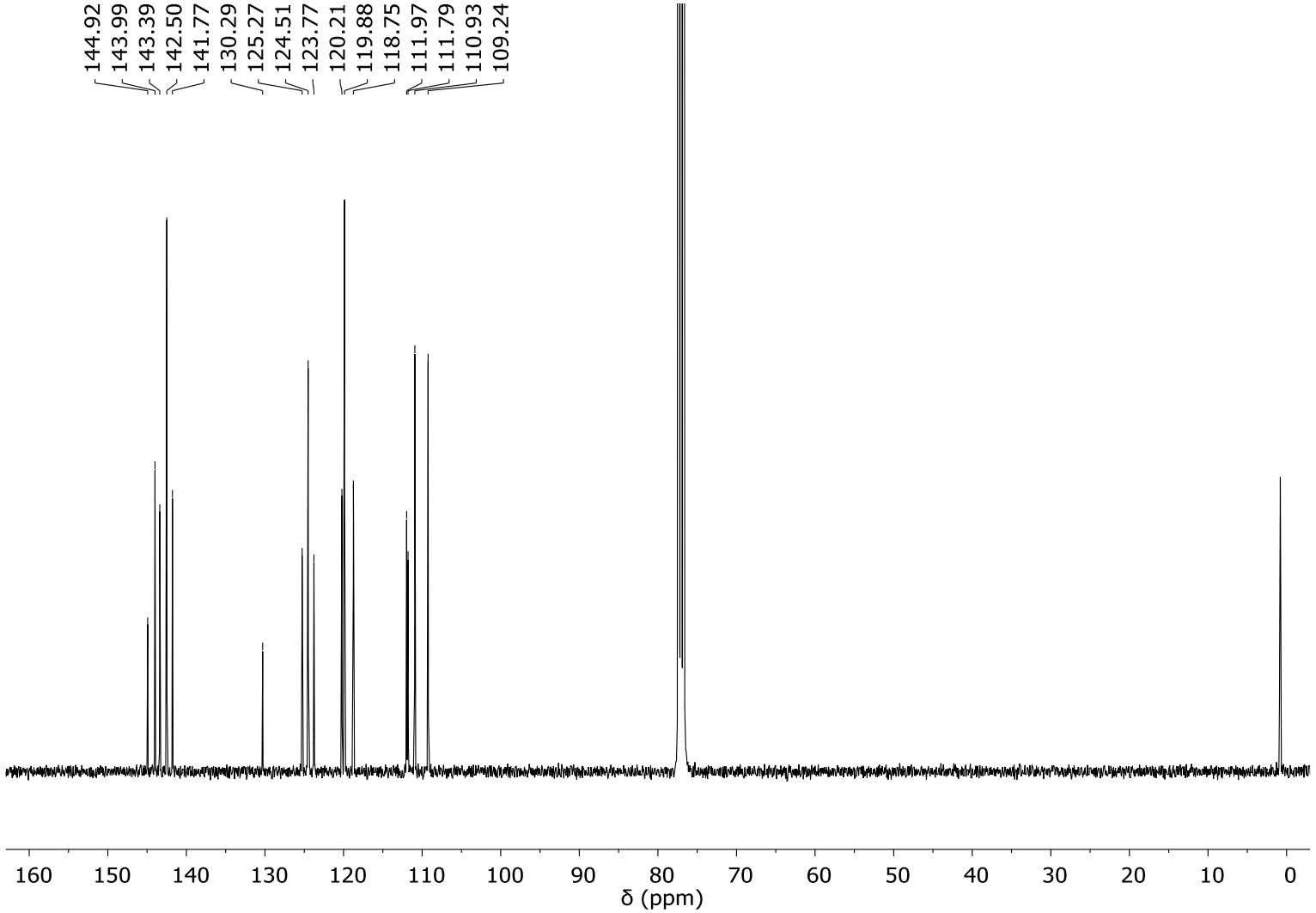

Figure S2: ^{13}C NMR spectrum of **4DTPIPN** in $CDCl_3$.

3. Photostability and thermostability

The photostability of both **4DTPIPN** and **4CzIPN** in neat film was measured in vacuum under constant irradiation from 355 nm light (Jobin Yvon Fluorolog) (Figure S3). The decrease in photoluminescence intensity was measured for approximately 4 hours. Due to the low photoluminescence quantum yield of **4DTPIPN** the signal to noise of the decay is very low which affects the R^2 value of the exponential fitting (Table S1).

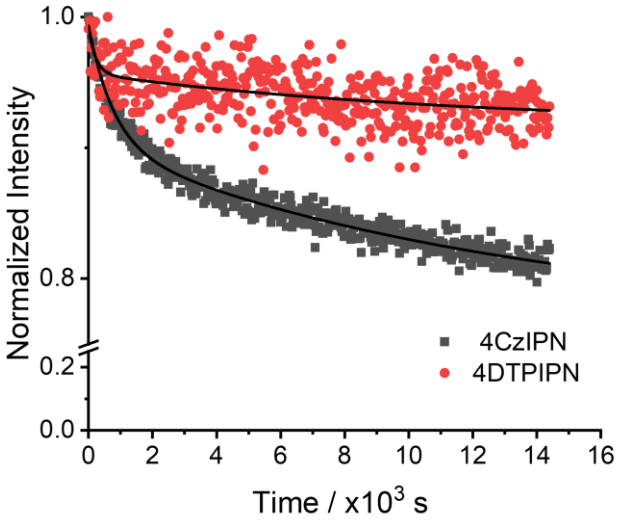

Figure S3: Photostability of **4DTPIPN** by measuring the decrease in emission intensity under constant irradiation over time. The photostability data were fitted using $y = y_0 + A_1 e^{(-(x-x_0)/t_1)} + A_2 e^{(-(x-x_0)/t_2)}$. The fitting parameters are included in Table S1.

Table S1: Fitting parameters for the fitting of the photostability curves in Figure S3.

	y_0	x_0	A_1	t_1	A_2	t_2	R^2
4DTPIPN	0.918±0.016	0	0.035±0.011	228±131	0.039±0.013	11400±8570	0.245
4CzIPN	0.766±0.013	0	0.090±0.004	781±64	0.137±0009	13100±2280	0.968

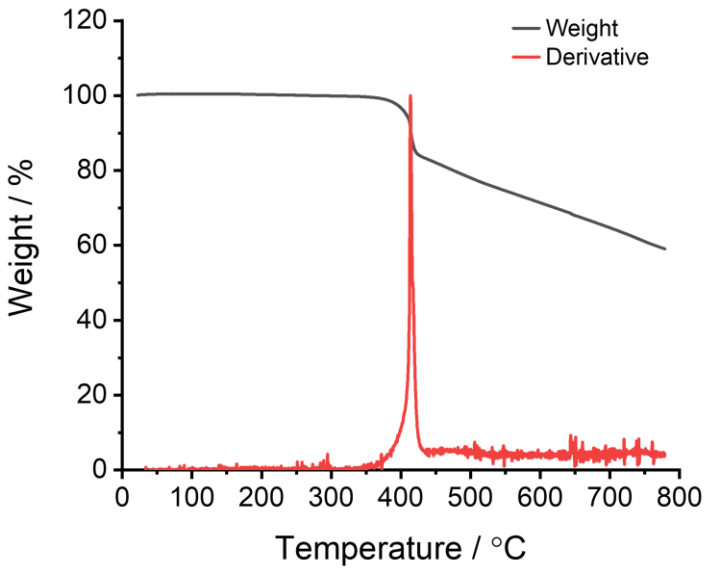

Figure S4: Thermal stability of **4DTPIPN** as measured via thermogravimetric analysis. Degradation of the product occurs above 414 °C.

The TGA measurement was performed using a TA Instruments (TGA 55; cycle from room temperature to 800 °C at 10 °C/min in a hT-Pt-pan (high temp. platina pan) under 10/90 N_2 (balance/sample) flow).

4. Crystal structures and additional calculations

Table S2: Interplanar angles between the benzene ring (A) and donor units (D1-4, scheme) in **4DTPIPN** and **4CzIPN,** from the X-ray structures.

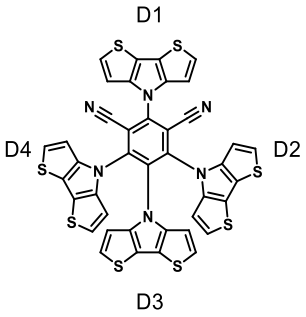

4DTPIPN

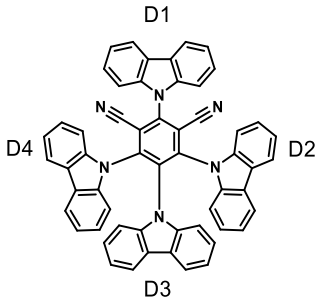

4CzIPN

		D1/A (°)	D2/A (°)	D3/A (°)	D4/A (°)
4DTPIPN	120 K	56.6(2)	58.5(3)	59.6(2)	55.5(2)
	220 K	57.4(3)	57.1(3)	59.9(3)	57.1(3)
4CzIPN[8]		53.8-72.6	56.7-72.3	60.6-67.9	52.3-74.6

4DTPIPN crystallised from acetonitrile as a **4DTPIPN**·4MeCN solvate, air-unstable at ambient temperature. At 220 K, the crystals are orthorhombic; *crystal data*: $C_{40}H_{16}N_6S_8 \cdot 4C_2H_3N$, f.w. 1001.28, a=32.319(4), b=10.7772(16), c=13.7517(18) Å, V=4789.8(11) Å^3, space group $C222_1$ (no. 20), Z=4, 33408 reflections (4326 unique, R_{int}=0.143) with 2θ≤50.8°, R_1=0.089 on 3482 reflections with $I \geq 2\sigma(I)$, wR_2=0.216 on all data. The molecule (Figure S5) lies on a crystallographic twofold axis passing through N(2), C(2), C(5) and N(5). The structure contains solvent-accessible voids of 1701 Å^3 per unit cell (35.6% of the crystal space) occupied by disordered MeCN. Between 220 and 200 K, a transition to a monoclinic structure occurs, accompanied by twinning. At 200 K, a=10.7914(15), b=13.755(2), c=16.983(2) Å, β=107.896(5)°, V=2399(1) Å^3. This phase was fully characterised at 120 K on a different crystal; c*rystal data*: a=10.6435(14), b=13.5768(15), c=16.7738(18) Å, β=107.252(5)°, V=2314.8(7) Å^3, space group $P2_1$ (no. 4), Z=2, 28550 reflections (8042 unique, R_{int}=0.105) with 2θ≤50°, twin law -1 0 0 0 -1 0 0.935 0 1 with the component ratio 0.820:0.180(4), R_1=0.080 on 6806 reflections with $I \geq 2\sigma(I)$, wR_2=0.181 on all data. The host molecule has no crystallographic symmetry but retains an approximate C_2 symmetry (Figure S5). At 120 K, the MeCN molecules were resolved at atomic approximation, whereas at 220 K they were intensely disordered and had to be masked using the OLEX SMTBX program based on the algorithm of Rees *et al*.[9] The structures have been deposited with the Cambridge Structural Database as CCDC-2095357 (120 K) and 2095358 (220 K).

The donor moieties are essentially planar. D2, D3, and D4 are inclined with respect to the acceptor benzene ring in a propeller-like fashion, while moiety D1 has an almost eclipsed orientation with respect to D3. The N(D)-C(A) bonds are practically coplanar with moieties D1 and D3, but are tilted out of the plane for the D2 and D4 planes by 14.0(6)° and 10.8(7)° at 120 K, and by 12.1(5)° at 220 K. Such conformation is also typical for **4CzIPN** in its various crystal forms;[8] the interplanar angles between donor and acceptor moieties in **4DTPIPN** are within the range observed in **4CzIPN** but close to the lower end of this range (Table S2).

Since the emission shifts in **4CzIPN** are attributed to the formation of dimers/aggregates via face-to-face overlap (π-π stacking) of carbazole moieties,[8] a comparative analysis of the crystal packing of **4DTPIPN** and **4CzIPN** is instructive. In principle, the D1 moiety and the *outer* faces of D2 and D4 are potential sites for π-π stacking. A contacting planar moiety can also wedge between D3 and D2 (or D4), forming a partial π-π overlap with one of these and a herring-bone ('π-σ') contact with the other, but this requires the D/A angles to be larger than 70°. In pristine (sublimed) solid **4CzIPN**, the D1 carbazole moieties forms infinite stacks, while both D2 and D4 participate in near-perpendicular π-σ contacts. In isostructural crystals of **4CzIPN**·3$CHCl_3$ and **4CzIPN**·3THF the host molecules form separate dimers via D1-D1 overlap, while the outer faces of D2 and D4 are masked by solvent molecules of crystallisation. A marginal D1-D1 overlap occurs also in **4CzIPN**·3.5Me_2CO,

while in **4CzIPN**·1.8MeCN and the mixed CH_2Cl_2/acetone/hexane solvate a 'wedging' dimerization occurs, with D1-D3 and D4-D4 intermolecular overlaps, respectively, with other potential stacking sites masked by solvent molecules or herring-bone oriented carbazole moieties.
In striking contrast, the crystal packing of **4DTPIPN**·4MeCN (essentially the same in both polymorphs, notwithstanding different space group symmetry) does not display any π-π overlaps between DTP moieties. Instead, the latter form peculiar edge-to-face synthons, in each case involving one close S…S contact (somewhat shorter than twice the van der Waals radius[10] of 1.8 Å) with two adjacent C-H bonds pointing towards the N atoms of the DTP and the cyano group, respectively (Figure S6, Table S3). The D1 moiety participates in four such contacts (two at faces and two at edges), while the D2 and D4 moieties participate in two contacts (one at face and one at edge) each. Relatively narrow D/A angles preclude wedging overlap (see Table S2), which in any case would be sterically unfavourable due to the large size of the sulphur atoms. The rest of the molecule's environment is dominated by eight somewhat longer S…S contacts (3.71–3.78 Å at 120 K, 3.76–3.78 Å at 220 K) between DTP moieties oriented edge-to-edge. The structures contain large enclosed voids (making up ca. 35% of the crystal space), each occupied by eight MeCN molecules. The latter do not mask any of the DTP faces effectively, in contrast to solvated **4CzIPN** structures.

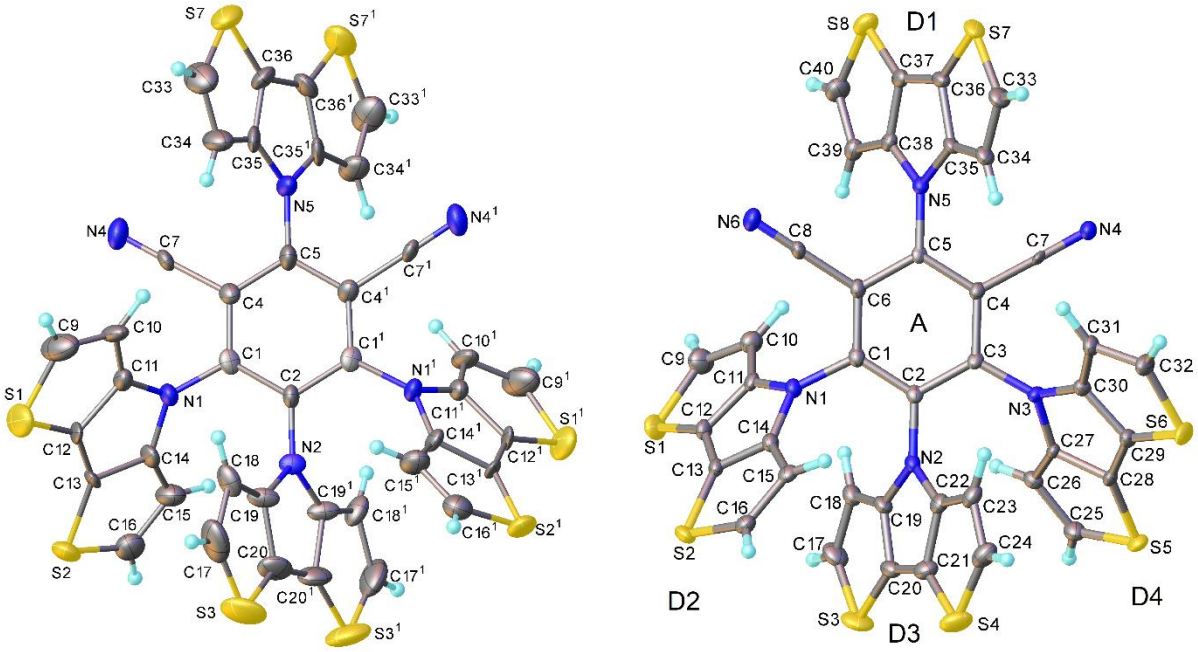

Figure S5: X-ray molecular structure of **4DTPIPN** in the orthorhombic (studied at 220 K, left, primed atoms are generated by the twofold axis) and monoclinic form (studied at 120 K, right). Atomic displacement ellipsoids are drawn at the 50% probability level. MeCN molecules of crystallisation are not shown.

Table S3: Intermolecular contacts (see Figure S6) between DTP moieties in the monoclinic **4DTPIPN**·4MeCN (in Å, C-H bond lengths normalised to 1.08 Å).

edge→face	S…S	H…N(DTP)	H…NC	face←edge	S…S	H…N(DTP)	H…NC
D1→D2(i)	3.45	2.65	2.68	D1←D2(iii)	3.43	3.00	2.90
D1→D4(ii)	3.49	2.54	2.66	D1←D4(iv)	3.41	3.24	3.05
D2→D1(i)	3.43	3.00	2.90	D2←D1(iv)	3.49	2.54	2.66
D4→D1(ii)	3.41	3.24	3.05	D1←D4(iii)	3.45	2.65	2.68

Symmetry transformations: (i) 1-x, y-1/2, 1-z; (ii) 2-x, y+1/2, 1-z; (iii) 1-x, y+1/2, 1-z; (iv) 2-x, y-1/2, 1-z

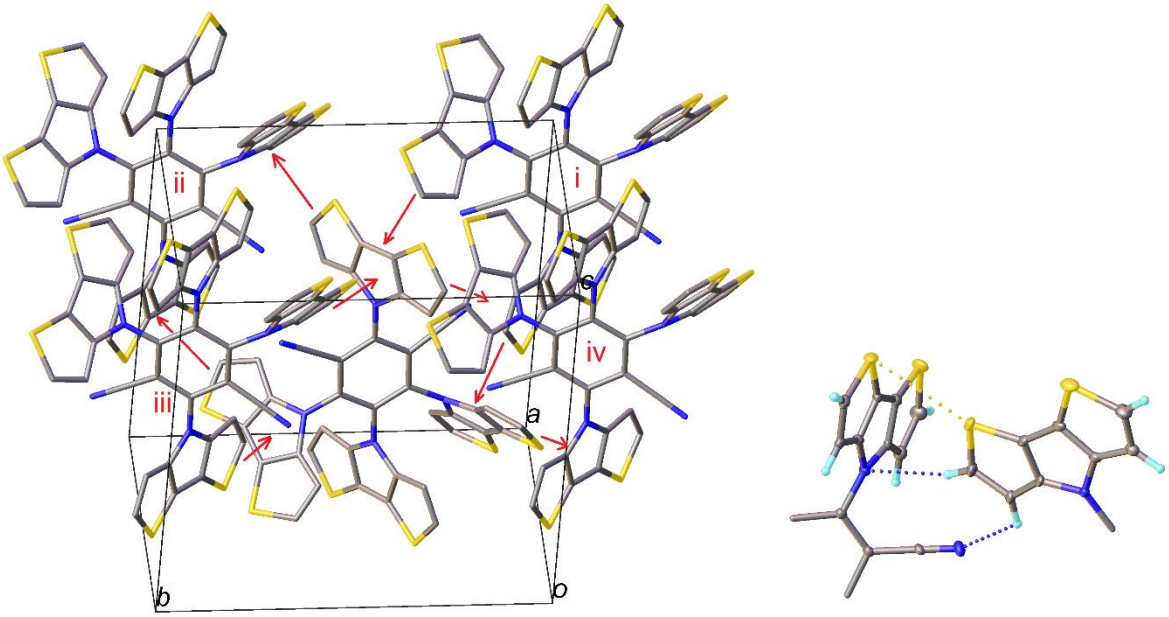

Figure S6: Left: crystal packing of **4DTPIPN** in the monoclinic polymorph. H atoms and solvent molecules are omitted for clarity. Red arrows show edge-to-face DTP-DTP contacts listed in Table S3. Symmetry transformations: (i) 1-x, y-1/2, 1-z; (ii) 2-x, y+1/2, 1-z; (iii) 1-x, y+1/2, 1-z; (iv) 2-x, y-1/2, 1-z. Right: a DTP-DTP contact in detail.

5. Frontier orbital topologies and energies

4DTPIPN

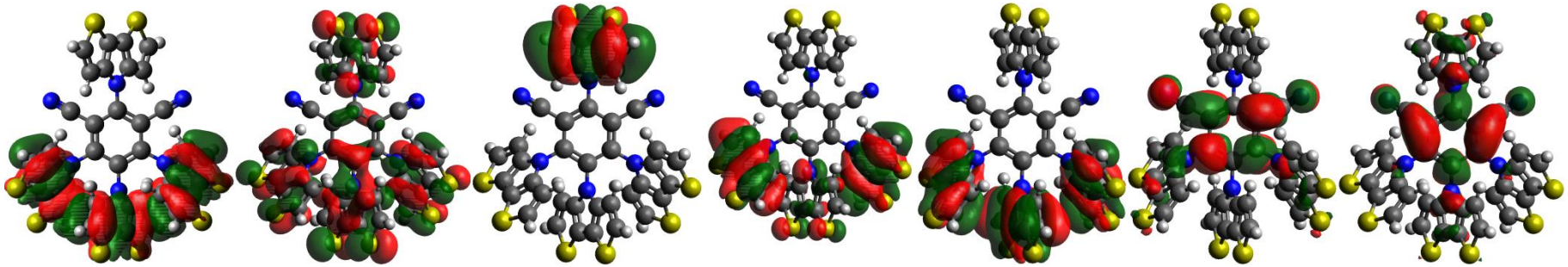

4CzIPN

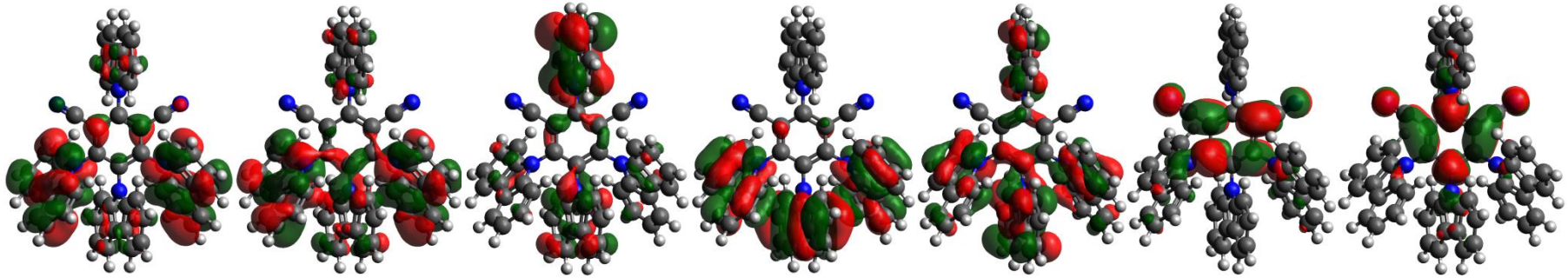

Figure S7: Orbital topologies for **4DTPIPN** and **4CzIPN** as obtained using LC-BLYP(ω=0.17 bohr^{-1})/6-311G(d) and the PCM (cyclohexane). Isosurface values of 0.02 a.u. were used for all orbitals.

Table S4: Orbital energies for the orbitals of **4DTPIPN** and **4CzIPN** shown in Figure S7 as obtained using LC-BLYP(ω=0.17 bohr^{-1})/6-311G(d) and the PCM (cyclohexane).

	HOMO-4 (eV)	HOMO-3 (eV)	HOMO-2 (eV)	HOMO-1 (eV)	HOMO (eV)	LUMO (eV)	LUMO+1 (eV)
4DTPIPN	-7.30	-7.27	-7.08	-7.06	-6.84	-1.45	-1.07
4CzIPN	-7.51	-7.45	-7.38	-7.34	-7.15	-1.36	-1.03

6. Steady-state absorption (solution and film) and emission (solution) spectra

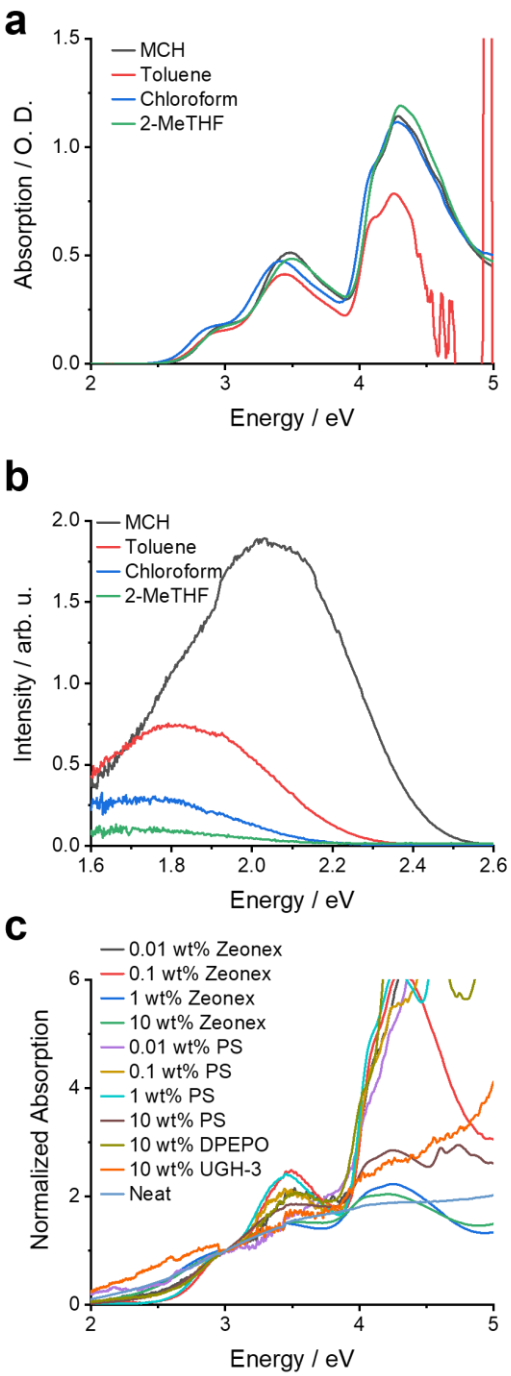

Figure S8: a) Steady-state absorption and b) fluorescence emission spectra for **4DTPIPN** in various solvents: methylcyclohexane (MCH), toluene, chloroform, and 2-methyltetrahydrofuran (2-MeTHF). c) Steady-state absorption of **4DTPIPN** in various host materials (polystyrene, zeonex, UGH-3, DPEPO, and neat) and at different concentrations (for polystyrene and zeonex).

7. Time-resolved emission spectra

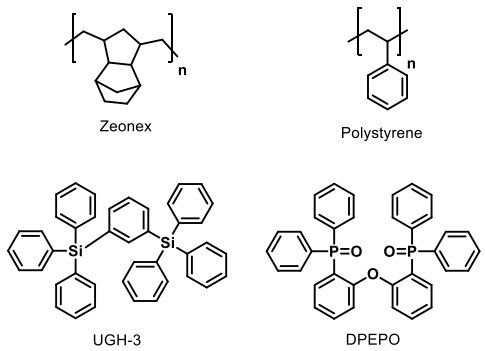

Figure S9: Molecular structures of zeonex, polystyrene, UGH-3, and DPEPO.

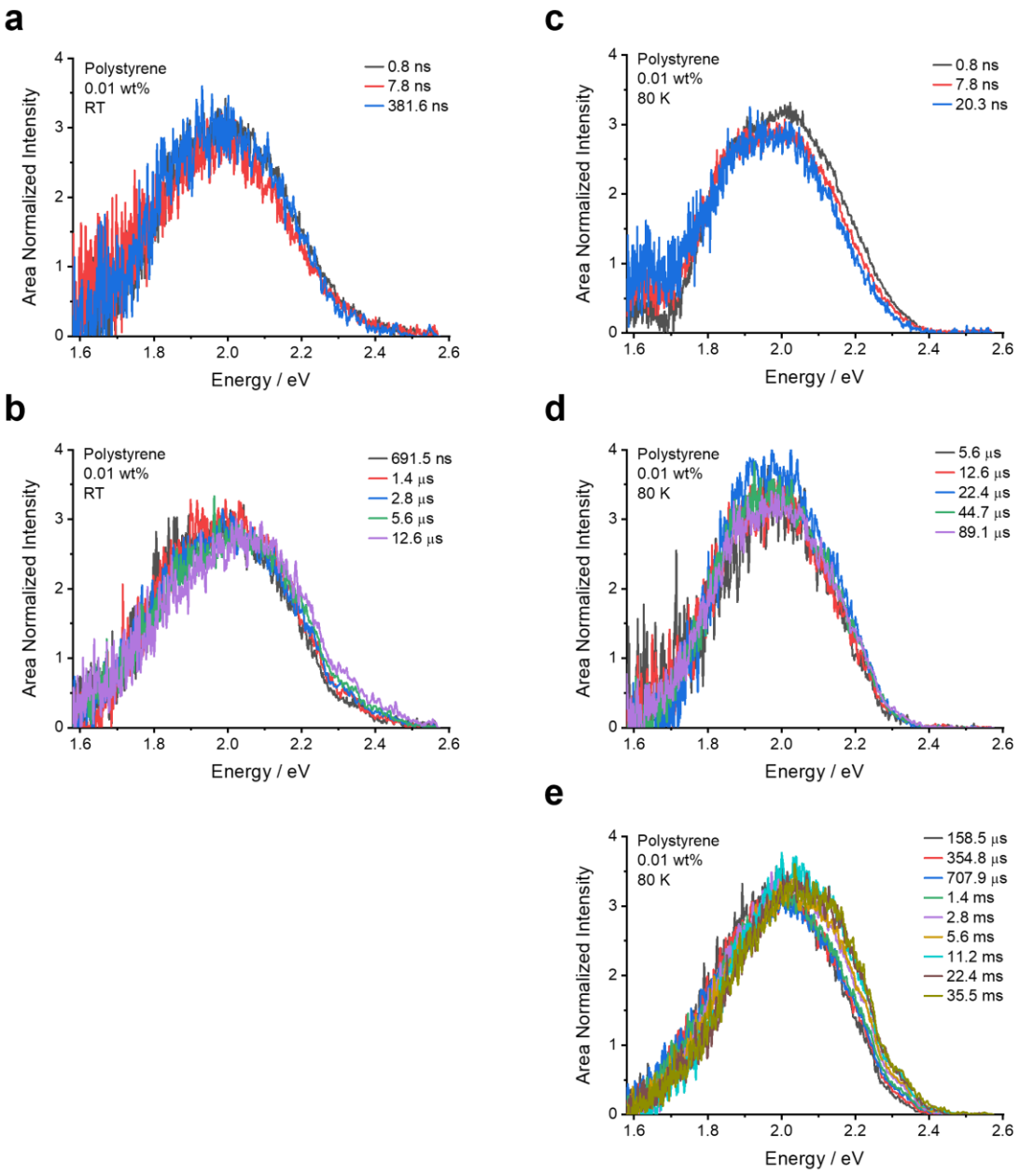

Figure S10: Emission spectra extracted from the time-resolved emission decay of **4DTPIPN** in a 0.01 wt% doped polystyrene film at room temperature (left) and 80 K (right).

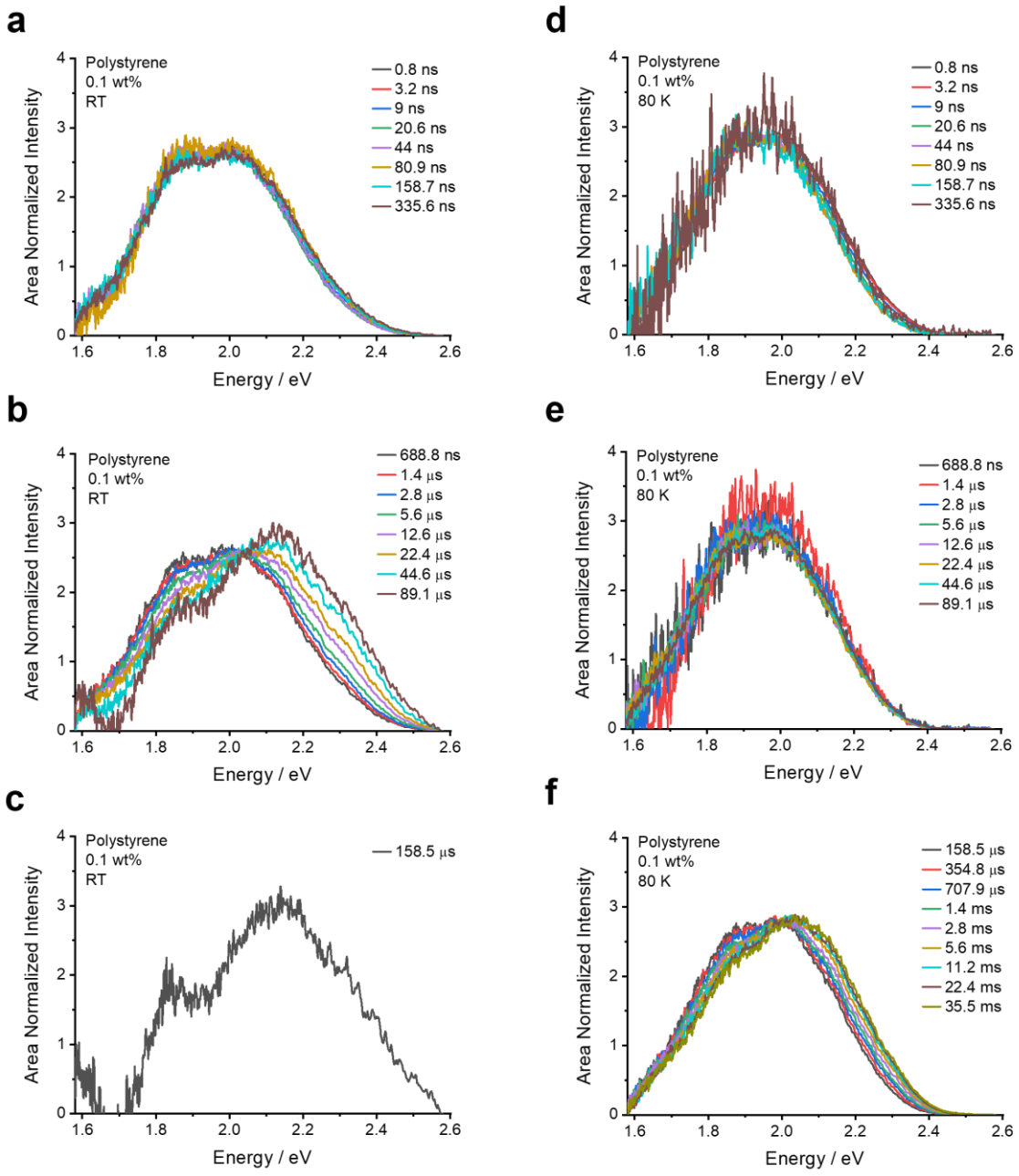

Figure S11: Emission spectra extracted from the time-resolved emission decay of **4DTPIPN** in a 0.1 wt% doped polystyrene film at room temperature (left) and 80 K (right).

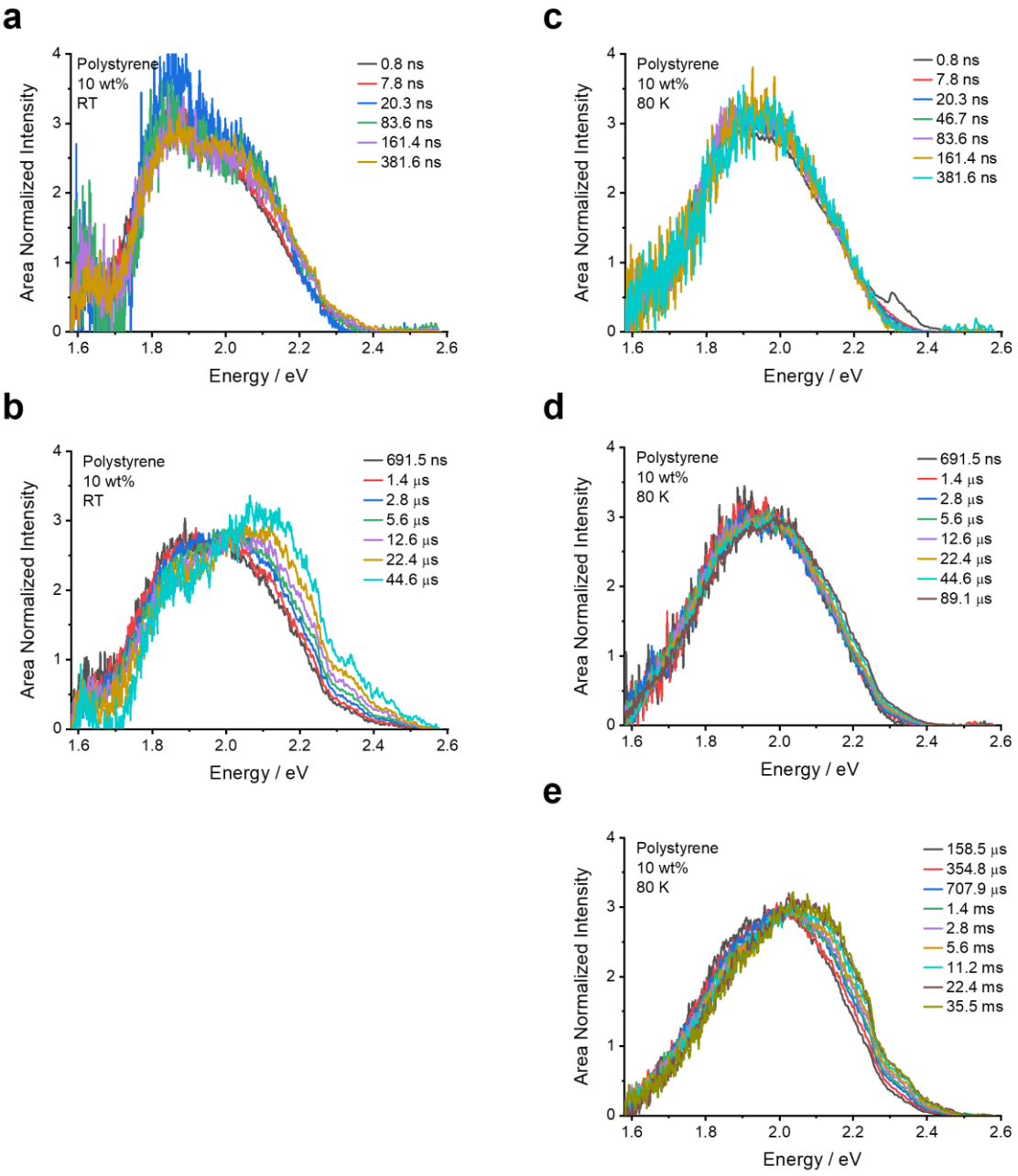

Figure S12: Emission spectra extracted from the time-resolved emission decay of **4DTPIPN** in a 10 wt% doped polystyrene (PS) film at room temperature (left) and 80 K (right).

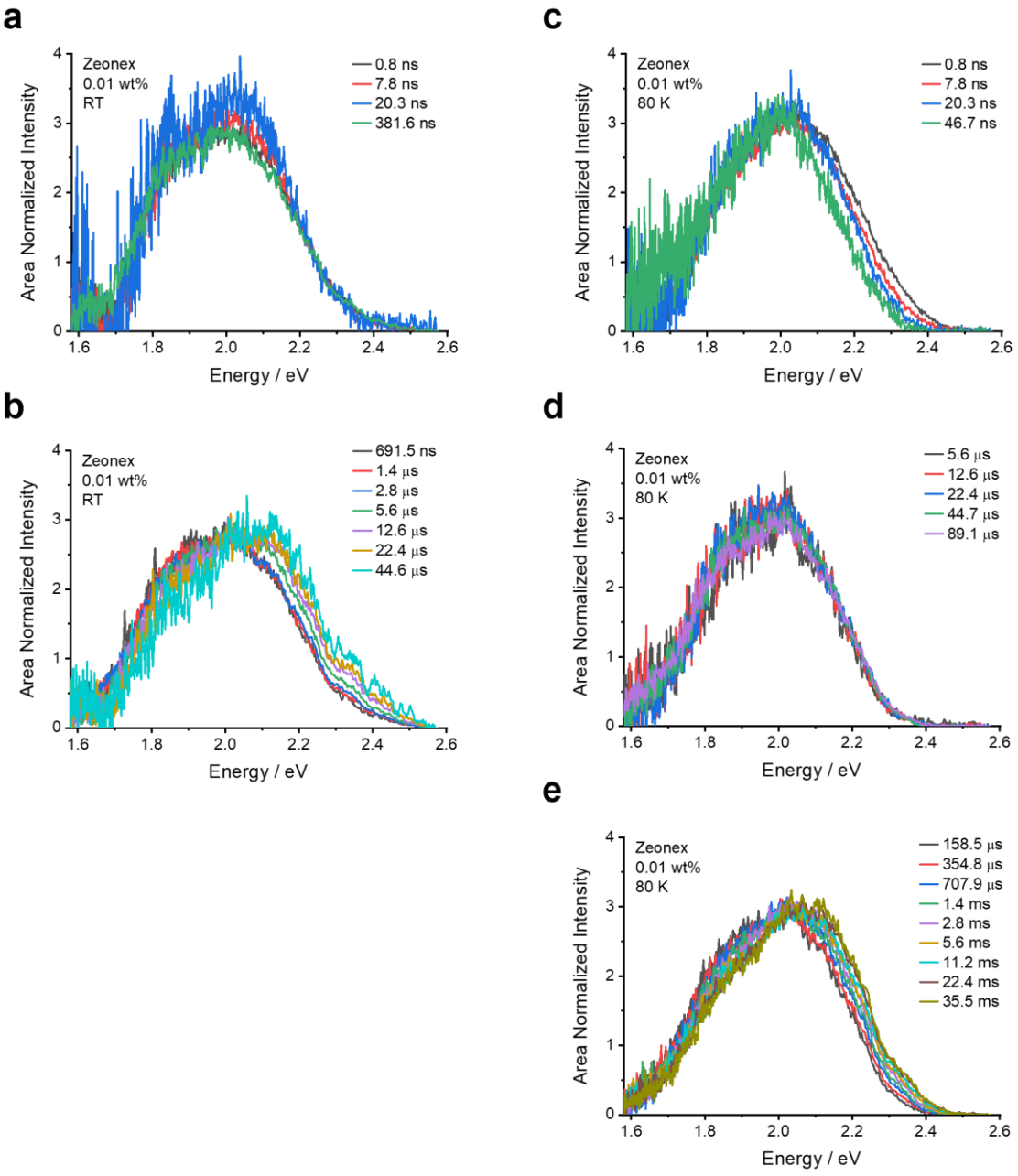

Figure S13: Emission spectra extracted from the time-resolved emission decay of **4DTPIPN** in a 0.01 wt% doped zeonex film at room temperature (left) and 80 K (right).

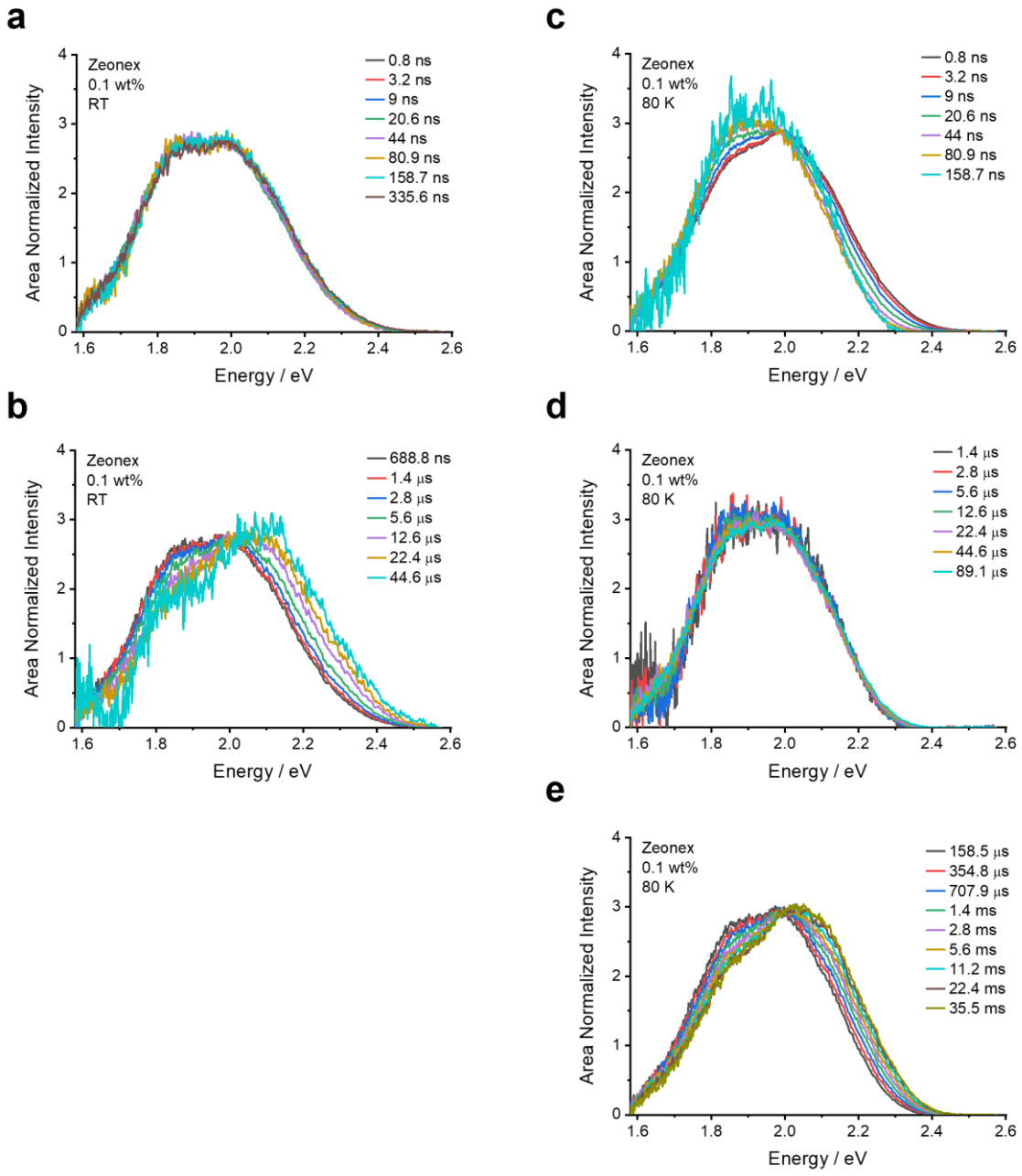

Figure S14: Emission spectra extracted from the time-resolved emission decay of **4DTPIPN** in a 0.1 wt% doped zeonex film at room temperature (left) and 80 K (right).

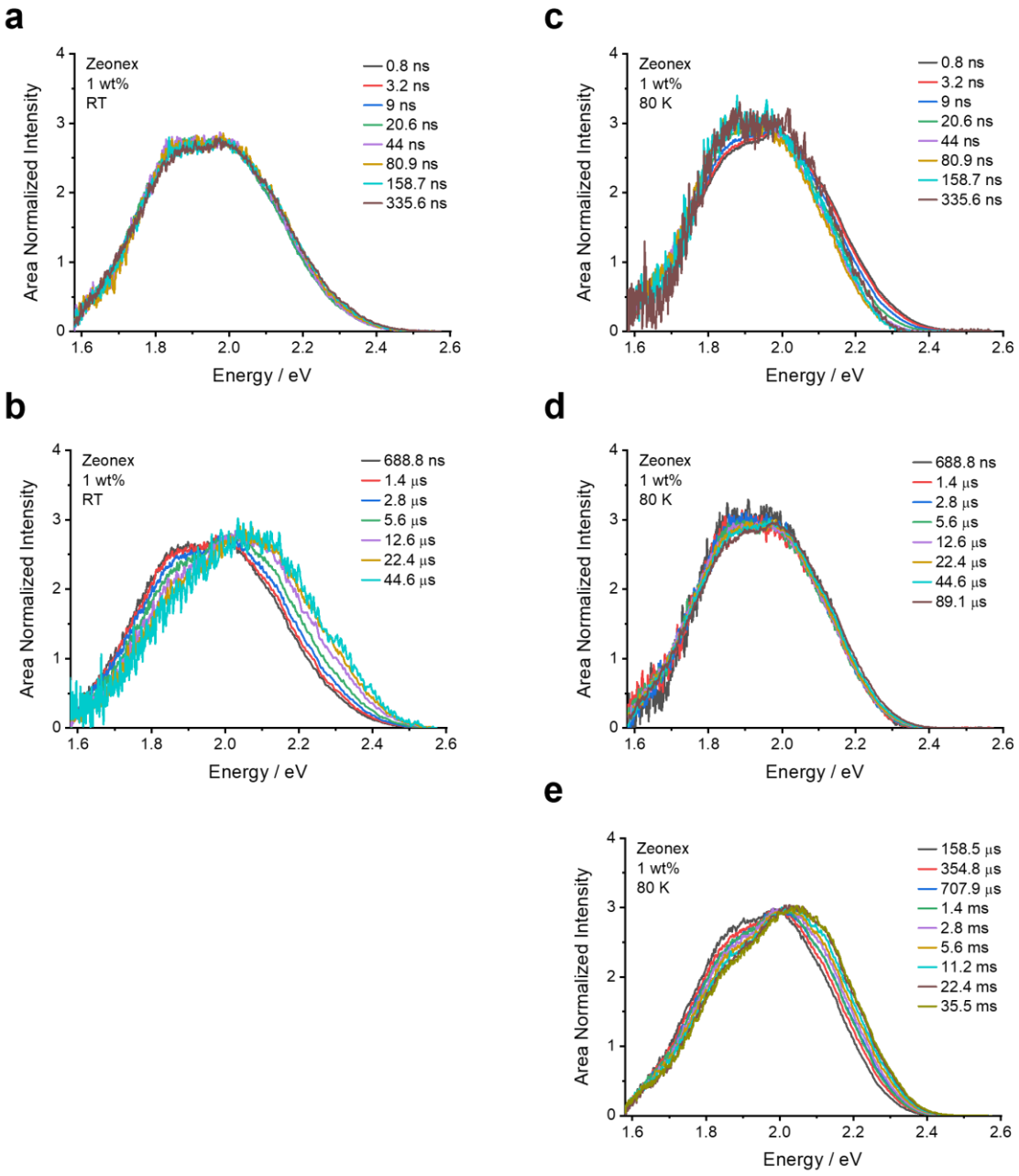

Figure S15: Emission spectra extracted from the time-resolved emission decay of **4DTPIPN** in a 1 wt% doped zeonex film at room temperature (left) and 80 K (right).

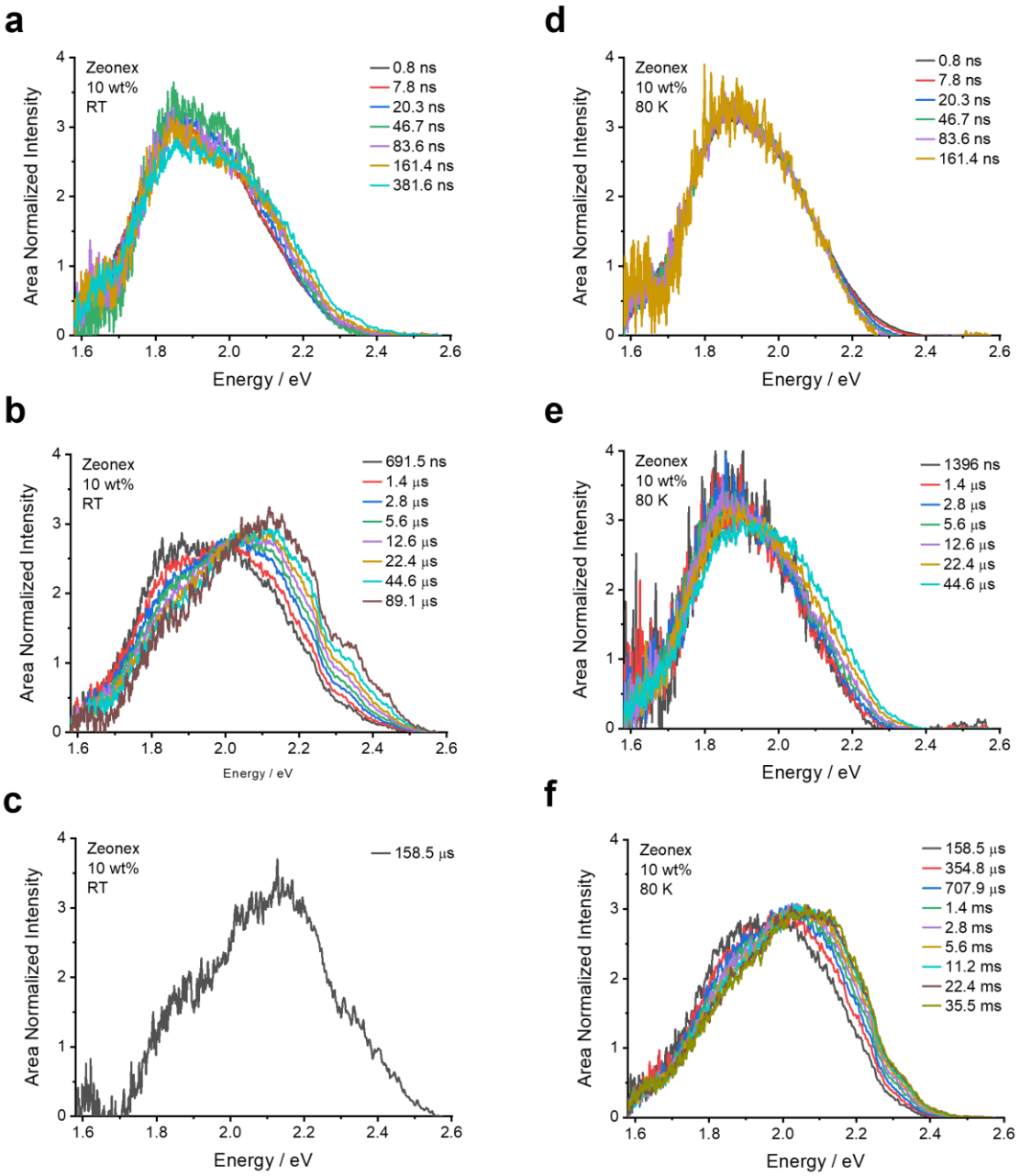

Figure S16: Emission spectra extracted from the time-resolved emission decay of **4DTPIPN** in a 10 wt% doped zeonex film at room temperature (left) and 80 K (right).

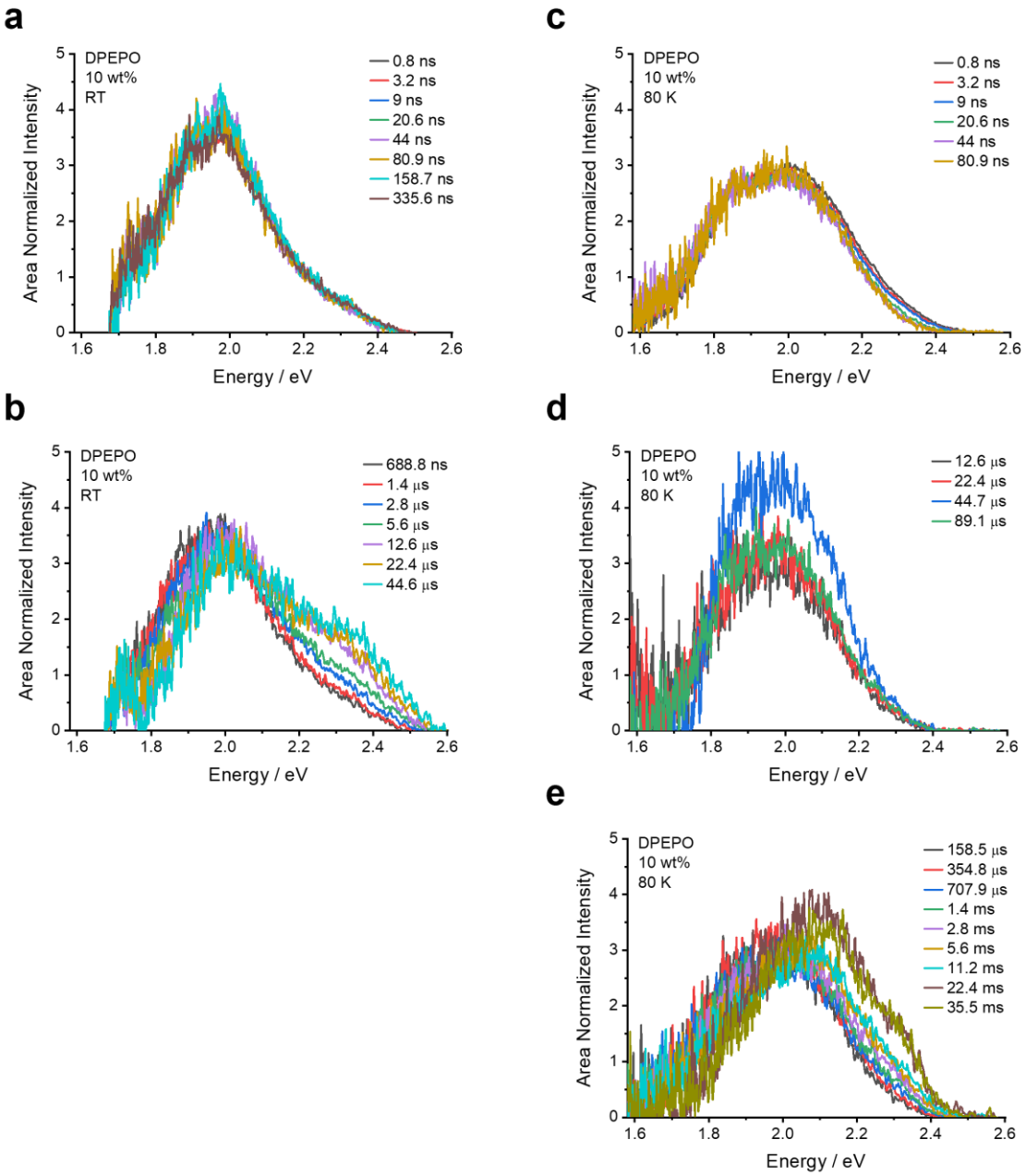

Figure S17: Emission spectra extracted from the time-resolved emission decay of **4DTPIPN** in a 10 wt% doped DPEPO film at room temperature (left) and 80 K (right).

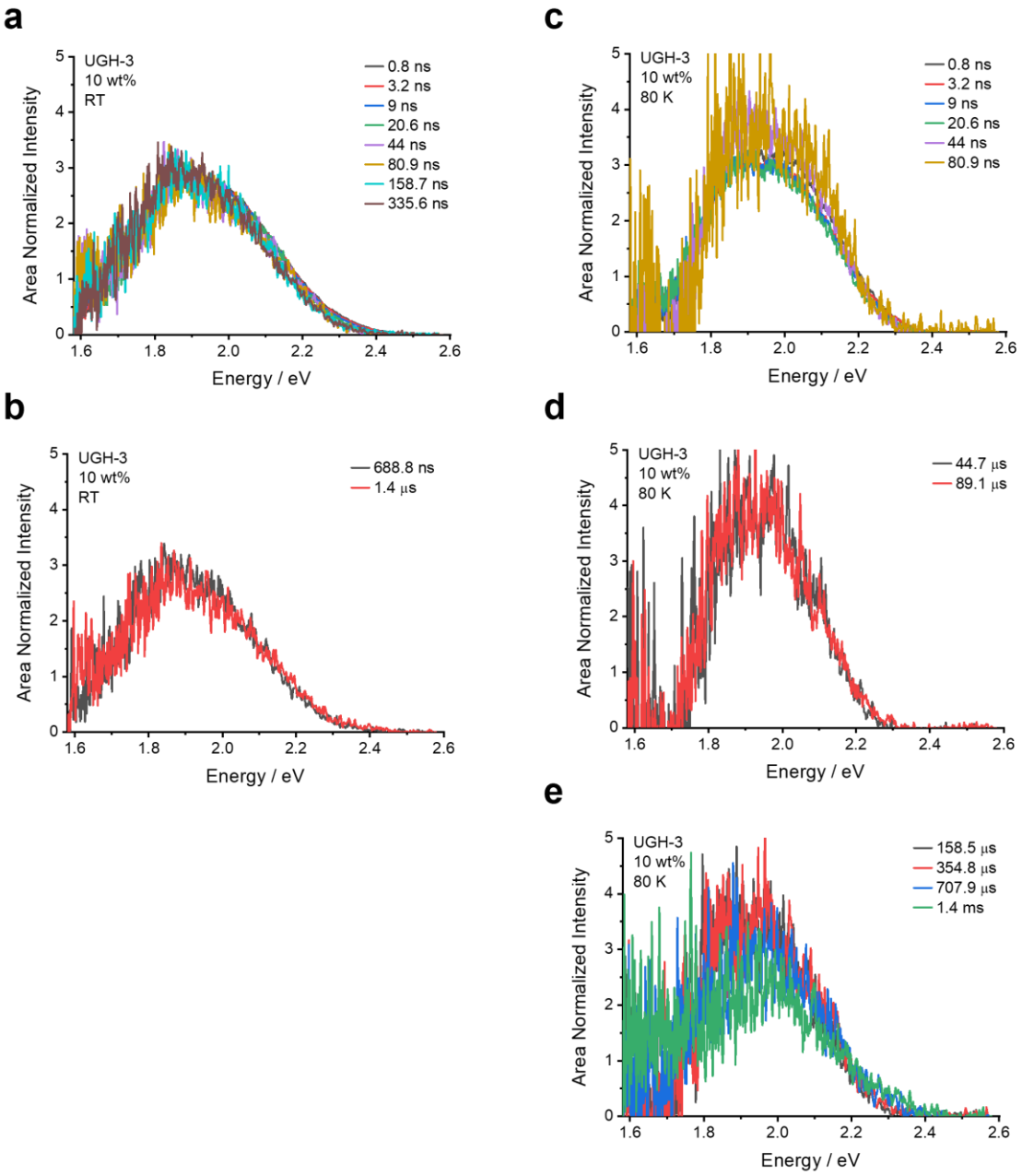

Figure S18: Emission spectra extracted from the time-resolved emission decay of **4DTPIPN** in a 10 wt% doped UGH-3 film at room temperature (left) and 80 K (right).

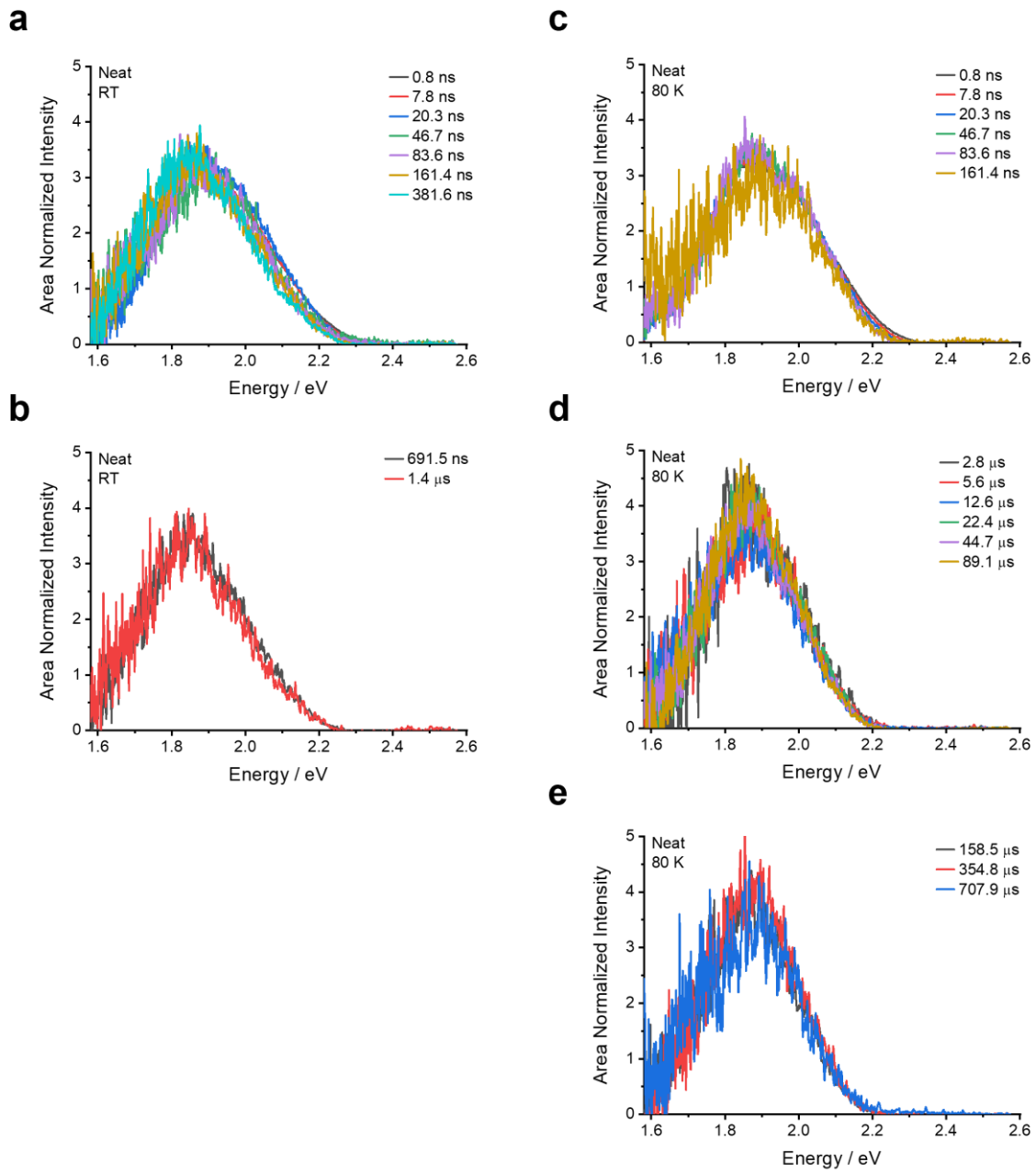

Figure S19: Emission spectra extracted from the time-resolved emission decay of a **4DTPIPN** neat film at room temperature (left) and 80 K (right).

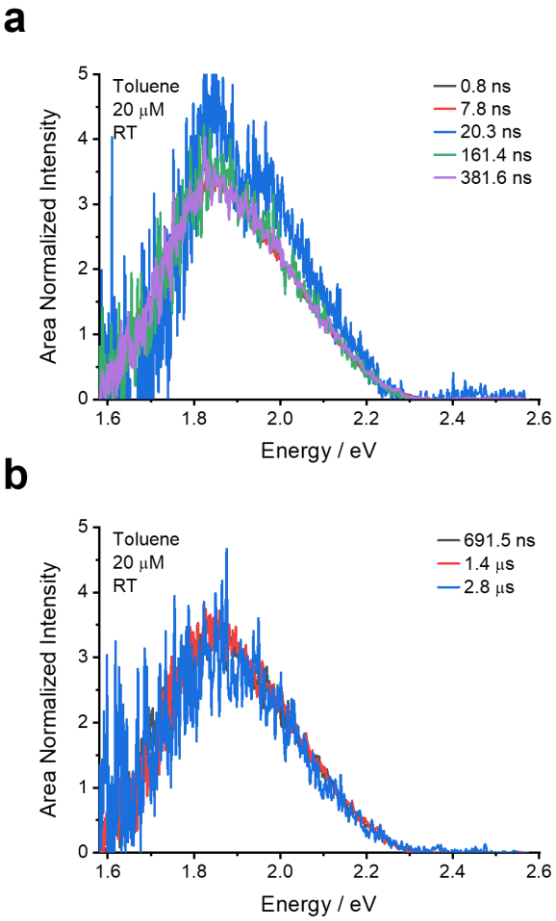

Figure S20: Emission spectra extracted from the time-resolved emission decay of **4DTPIPN** in toluene solution (20 μM concentration) at room temperature.

8. Laser energy measurements

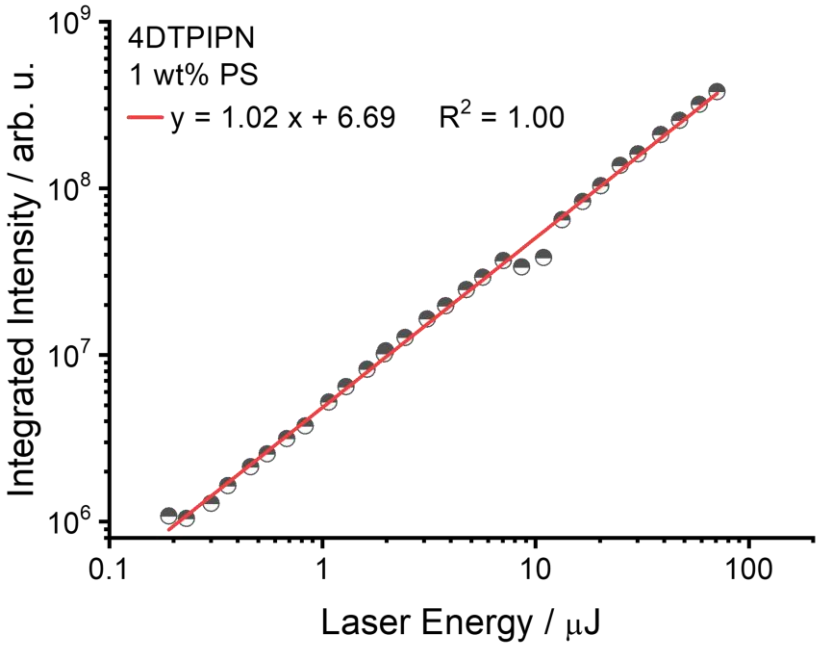

Figure S21: Integrated intensity versus laser energy for a 1 wt% polystyrene film of **4DTPIPN** measured at a 3 μs delay time and a 20 μs integration time. A slope near 1 is indicative of TADF behaviour.

9. Singlet oxygen quantum yield

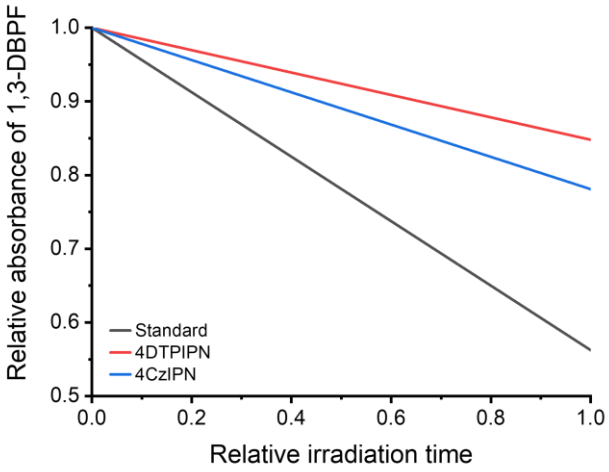

Figure S22: Absorbance of 1,3-diphenylisobenzofuran at 414 nm over time while the sample is irradiated with a 325 nm LED. The sample contains either **4DTPIPN**, **4CzIPN**, or the coronene standard as the photosensitizer.

10. Kinetic fits

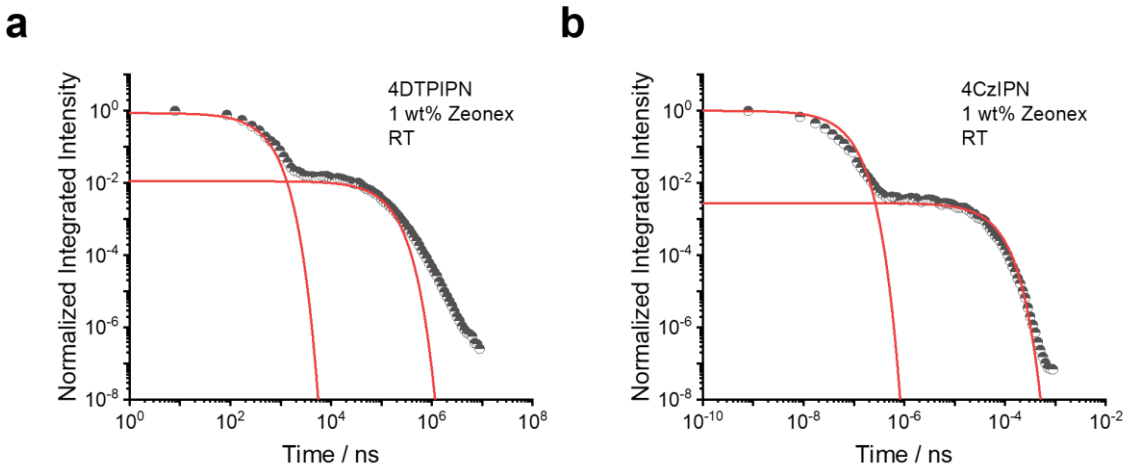

Figure S23: Exponential fits of the emission decays in 1 wt% zeonex film for **4DTPIPN** and **4CzIPN** (for comparison) according to the kinetic fitting model introduced by N. Haase *et al.*[11]

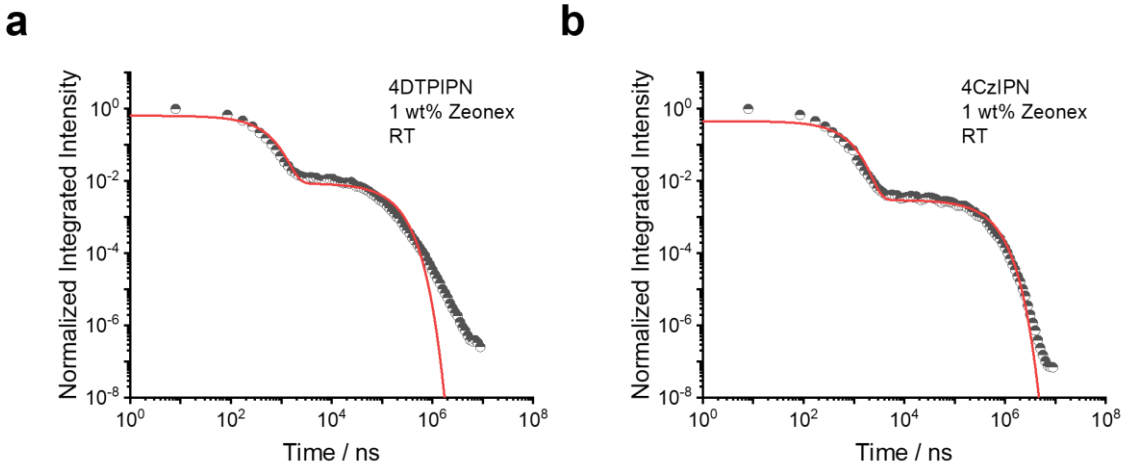

Figure S24: Kinetic fits of the emission decays in 1 wt% zeonex film for **4DTPIPN** and **4CzIPN** (for comparison) according to the kinetic fitting model introduced by N. Haase *et al.*[11]

The kinetic parameters ($\tau_{PF}, \tau_{DF}, k_F, k_{ISC}$ and k_{rISC}) were obtained according to exponential fitting and the kinetic fitting model introduced by N. Haase *et al.*[11] For the non-radiative decay rate of the singlet state (k_{nr}^S) we used Equation 85 from the work by Tsuchiya *et al.* [12]

$$k_{nr}^S = k_P \frac{\Phi_{PF}}{\Phi_{PLQY}}(1 - \Phi_{PLQY})$$

Where k_P is the prompt decay rate ($k_P = \frac{1}{\tau_{PF}}$), Φ_{PF} is the yield of the prompt fluorescence and is taken to be the PLQY of the sample in air, Φ_{PLQY} is the total yield and is taken to be the PLQY of the sample under nitrogen.

For the 1 wt% zeonex films of interest in air and (under nitrogen) PLQYs of **4DTPIPN** and **4CzIPN** are 3.5% (4.5%) and 54% (87%), respectively.[13] This gives the values as detailed in Table S5. The order of magnitude difference in the rates between **4DTPIPN** and **4CzIPN** is consistent with the TADF performance of the two compounds. While **4DTPIPN** has a slightly higher rISC rate and similar prompt fluorescence lifetime the overall performance of the compound is limited by its low PLQY and high non-radiative decay rate.

Table S5: Kinetic parameters (τ_{PF},τ_{DF},k_F,k_{ISC} and k_{rISC}) obtained from exponential fitting (lifetimes, Figure S23) and the kinetic fitting procedure of the emission decays of **4DTPIPN** and **4CzIPN** as applied in Figure S24. k_{nr}^S was obtained according to equation 85 in a study by Tsuchiya *et al*.[12]

	$\boldsymbol{\tau_{PF}}$/ns	$\boldsymbol{\tau_{DF}}$/10^3 ns	$\boldsymbol{k_F}$/10^6	$\boldsymbol{k_{ISC}}$/10^7	$\boldsymbol{k_{rISC}}$/10^5	$\boldsymbol{k_{nr}^S}$/10^6
4DTPIPN	30.03±0.24	8.30±0.21	4.677±0.005	1.82±0.04	3.90±0.00[a]	24.8±44.8[b]
4CzIPN	40.50±0.53	40.04±0.86	3.28±0.46	1.33±0.08	1.37±0.10	2.02±0.22

[a] The error is zero for several orders of magnitude on this value. [b] The large error value is a result of the low PLQY values for **4DTPIPN** which amplifies the relative error on the value.

11. Coordinates of optimized geometries

4DTPIPN

C	0.31593	-1.16290	-0.34644
C	-0.39206	0.00001	0.00001
C	0.31587	1.16295	0.34647
C	1.72037	1.15729	0.35022
C	2.42811	0.00008	0.00005
C	1.72044	-1.15717	-0.35015
C	2.42087	-2.30016	-0.83224
N	2.98234	-3.22664	-1.22812
C	2.42074	2.30033	0.83231
N	2.98216	3.22683	1.22818
N	3.82283	0.00011	0.00007
C	4.65547	0.86799	-0.71020
C	5.97854	0.55013	-0.44710
C	5.97855	-0.55000	0.44708
C	4.65549	-0.86780	0.71028
S	7.04345	-1.55311	1.36308
C	5.68424	-2.36992	2.07876
C	4.47853	-1.90591	1.65198
C	4.47849	1.90611	-1.65188
C	5.68419	2.37008	-2.07874
S	7.04342	1.55321	-1.36317
N	-1.79101	-0.00003	0.00001
C	-2.62127	0.83282	-0.74735
C	-3.94559	0.53241	-0.46697
C	-3.94557	-0.53259	0.46695
C	-2.62123	-0.83293	0.74734
S	-5.00829	-1.47731	1.44674
C	-3.64602	-2.24790	2.21059
C	-2.44116	-1.80937	1.75390
C	-2.44124	1.80928	-1.75389
C	-3.64612	2.24774	-2.21061
S	-5.00836	1.47706	-1.44678
N	-0.36070	-2.32671	-0.72574
C	-1.44216	-2.40782	-1.60674
C	-2.10005	-3.61347	-1.42369
C	-1.40988	-4.31869	-0.40536
C	-0.35737	-3.51956	0.00918
S	-1.52697	-5.73358	0.57543
C	-0.15958	-5.21556	1.51816
C	0.36603	-4.02662	1.11148
C	-1.97227	-1.60176	-2.63872
C	-3.05235	-2.20495	-3.20428
S	-3.42306	-3.76338	-2.52088
N	-0.36084	2.32673	0.72575
C	-1.44231	2.40779	1.60674
C	-2.10025	3.61342	1.42367
C	-1.41010	4.31866	0.40535
C	-0.35755	3.51958	-0.00918
S	-1.52724	5.73354	-0.57545
C	-0.15982	5.21557	-1.51817
C	0.36584	4.02666	-1.11148
C	-1.97240	1.60172	2.63872
C	-3.05251	2.20485	3.20426
S	-3.42328	3.76327	2.52085
H	5.87149	-3.17585	2.77655
H	3.52806	-2.29856	1.99753
H	3.52801	2.29882	-1.99736
H	5.87143	3.17601	-2.77654
H	-3.82969	-3.01794	2.94912

H	-1.49112	-2.19239	2.11463
H	-1.49122	2.19236	-2.11461
H	-3.82982	3.01777	-2.94914
H	0.20694	-5.86465	2.30313
H	1.23521	-3.56828	1.57176
H	-1.59754	-0.63206	-2.94879
H	-3.67839	-1.82436	-4.00126
H	0.20667	5.86467	-2.30314
H	1.23504	3.56835	-1.57175
H	-1.59763	0.63203	2.94879
H	-3.67854	1.82425	4.00123

4CzIPN

C	-0.24202	1.13518	-0.44212
C	0.46683	-0.00024	0.00010
C	-0.23916	-1.13728	0.44270
C	-1.64361	-1.11836	0.46242
C	-2.34619	-0.00338	0.00118
C	-1.64641	1.11307	-0.46087
C	-2.37676	2.19184	-1.03961
N	-2.97965	3.05166	-1.51582
C	-5.90338	0.46485	0.54901
C	-5.90304	-0.47108	-0.54934
C	-4.55928	-0.74006	-0.86211
N	-3.74595	-0.00476	0.00190
C	-4.55981	0.73206	0.86409
C	-6.90768	-1.08485	-1.29043
C	-6.55670	-1.94222	-2.31880
C	-5.21480	-2.18641	-2.61909
C	-4.19509	-1.58728	-1.89712
C	4.02837	0.56248	0.45421
C	4.02932	-0.55493	-0.45633
C	2.68748	-0.86971	-0.72657
N	1.86641	0.00134	-0.00032
C	2.68600	0.87426	0.72534
C	2.33492	1.86190	1.63312
C	3.35734	2.58076	2.23103
C	4.69723	2.30730	1.94747
C	5.03914	1.29162	1.07122
C	5.04130	-1.28181	-1.07406
C	4.70106	-2.29821	-1.95012
C	3.36159	-2.57465	-2.23278
C	2.33798	-1.85810	-1.63414
C	2.15965	3.55166	-1.65821
C	1.45672	4.31266	-0.65463
C	0.39245	3.51853	-0.19845
N	0.42275	2.28632	-0.88024
C	1.49685	2.32114	-1.78377
C	1.88749	1.37096	-2.71276
C	3.01079	1.64230	-3.47678
C	3.70732	2.84437	-3.33738
C	3.27809	3.81031	-2.44323
C	1.67373	5.56266	-0.08621
C	0.83526	5.99631	0.92627
C	-0.21433	5.19147	1.37122
C	-0.45114	3.94291	0.81693
C	-2.37104	-2.19908	1.04119
N	-2.97142	-3.06074	1.51727
C	2.16849	-3.54809	1.65834
C	1.46702	-4.31088	0.65509
C	0.40085	-3.51923	0.19900
N	0.42858	-2.28682	0.88050

C	1.50295	-2.31903	1.78378
C	1.89167	-1.36775	2.71245
C	3.01574	-1.63640	3.47629
C	3.71493	-2.83693	3.33701
C	3.28769	-3.80403	2.44317
C	1.68660	-5.56055	0.08692
C	0.84878	-5.99631	-0.92517
C	-0.20270	-5.19390	-1.37005
C	-0.44208	-3.94572	-0.81603
C	-4.19630	1.57917	1.89945
C	-5.21646	2.17987	2.61947
C	-6.55817	1.93727	2.31698
C	-6.90849	1.08006	1.28827
H	-7.95446	-0.88930	-1.06581
H	-7.33213	-2.42928	-2.90455
H	-4.96343	-2.85788	-3.43656
H	-3.15026	-1.76576	-2.14494
H	1.29700	2.07755	1.87467
H	3.10486	3.37375	2.93137
H	5.47694	2.89133	2.43017
H	6.08363	1.06225	0.86859
H	6.08541	-1.05011	-0.87212
H	5.48174	-2.88048	-2.43336
H	3.11040	-3.36817	-2.93298
H	1.30038	-2.07603	-1.87498
H	1.34210	0.43979	-2.84123
H	3.35268	0.90014	-4.19479
H	4.58649	3.02732	-3.95013
H	3.80632	4.75755	-2.35336
H	2.49941	6.18398	-0.42782
H	0.99087	6.97259	1.37837
H	-0.86796	5.55099	2.16219
H	-1.27777	3.33261	1.17308
H	1.34422	-0.43779	2.84085
H	3.35611	-0.89331	4.19407
H	4.59465	-3.01777	3.94961
H	3.81804	-4.75010	2.35340
H	2.51374	-6.17997	0.42846
H	1.00640	-6.97238	-1.37706
H	-0.85576	-5.55507	-2.16074
H	-1.27012	-3.33729	-1.17210
H	-3.15165	1.75629	2.14905
H	-4.96562	2.85127	3.43716
H	-7.33396	2.42550	2.90128
H	-7.95514	0.88584	1.06188

12. Supporting references

1. F. Wilkinson, W. P. Helman and A. B. Ross, *J. Phys. Chem. Ref. Data*, 1993, **22**, 113-262.
2. R. W. Redmond and J. N. Gamlin, *Photochem. and Photobiol.*, 1999, **70**, 391-475.
3. G. Sheldrick, *Acta Crystallogr. A*, 2015, **71**, 3-8.
4. G. Sheldrick, *Acta Crystallogr. C*, 2015, **71**, 3-8.
5. O. V. Dolomanov, L. J. Bourhis, R. J. Gildea, J. A. K. Howard and H. Puschmann, *J. Appl. Crystallogr.*, 2009, **42**, 339-341.
6. S. Förtsch, A. Vogt and P. Bäuerle, *J. Phys. Org. Chem.*, 2017, **30**, e3743.
7. S. Förtsch and P. Bäuerle, *Polym. Chem.*, 2017, **8**, 3586-3595.
8. M. K. Etherington, N. A. Kukhta, H. F. Higginbotham, A. Danos, A. N. Bismillah, D. R. Graves, P. R. McGonigal, N. Haase, A. Morherr, A. S. Batsanov, C. Pflumm, V. Bhalla, M. R. Bryce and A. P. Monkman, *J. Phys. Chem. C*, 2019, **123**, 11109-11117.
9. B. Rees, L. Jenner and M. Yusupov, *Acta Crystallogr. D*, 2005, **61**, 1299-1301.
10. S. S. Batsanov, *Inorg. Mater.*, 2001, **37**, 871.
11. N. Haase, A. Danos, C. Pflumm, A. Morherr, P. Stachelek, A. Mekic, W. Brütting and A. P. Monkman, *J. Phys. Chem. C*, 2018, **122**, 29173-29179.
12. Y. Tsuchiya, S. Diesing, F. Bencheikh, Y. Wada, P. L. dos Santos, H. Kaji, E. Zysman-Colman, I. D. W. Samuel and C. Adachi, *J. Phys. Chem. A*, 2021, **125**, 8074-8089.
13. M. K. Etherington, N. A. Kukhta, H. F. Higginbotham, A. Danos, A. N. Bismillah, D. R. Graves, P. R. McGonigal, N. Haase, A. Morherr, A. S. Batsanov, C. Pflumm, V. Bhalla, M. R. Bryce and A. P. Monkman, *J. Phys. Chem. C*, 2019, **123**, 11109-11117.